Continental Shelf Research 143 (2017) 257–270

Contents lists available at ScienceDirect

Continental Shelf Research

journal homepage: www.elsevier.com/locate/csr

Research papers

Interannual variation of spring phytoplankton bloom and response to turbulent energy generated by atmospheric forcing in the central Southern Yellow Sea of China: Satellite observations and numerical model study

Jie Shi[a,b], Yi Liu[c,d], Xinyan Mao[e], Xinyu Guo[a,b,f], Hao Wei[g], Huiwang Gao[a,b,*]

[a] Key laboratory of Marine Environment and Ecology, Ocean University of China, Ministry of Education, 238 Songling Road, Qingdao 266100, China
[b] College of Environmental Science and Engineering, Ocean University of China, 238 Songling Road, Qingdao 266100, China
[c] State Key Laboratory of Tropical Oceanography, South China Sea Institute of Oceanology, Chinese Academy of Sciences, 164 West Xingang Road, Guangzhou 510301, China
[d] University of Chinese Academy of Sciences, Beijing 100049, China
[e] College of Oceanic and Atmospheric Sciences, Ocean University of China, 238 Songling Road, Qingdao 266100, China
[f] Center for Marine Environmental Studies, Ehime University, 2-5 Bunkyo-Cho, Matsuyama 790-8577, Japan
[g] School of Marine Science and Technology, Tianjin University, Tianjin 300072, China

ARTICLE INFO

Keywords:
Spring phytoplankton bloom
Start timing
Magnitude
Duration
Turbulent kinetic energy
the central Southern Yellow Sea

ABSTRACT

The interannual variations of the start timing, magnitude and duration of the spring phytoplankton bloom (SPB) in the central southern Yellow Sea (SYS) were studied using the satellite-derived surface chlorophyll-*a* concentrations (Chl-*a*) from 2000 to 2014. The correlations between the characteristics of SPB and the generation rate of turbulent kinetic energy (TKE_{RT}) supplied from the atmosphere to the ocean were examined. The start timing of SPB was delayed in years with high TKE_{RT} supplied to the ocean before SPB. The TKE_{RT} during SPB had no relationship with the magnitude of SPB, but had positive correlation with the duration. A 1-D physical-biological model was used to examine the influencing mechanisms of the TKE_{RT} on the characteristics of SPB quantitatively. The wind speeds and related TKE_{RT} before the start of SPB were stronger in 2010 than in 2008. Comparison of the model results forced by winds in the two years suggested that the enhanced physical dilution of phytoplankton caused by the stronger TKE_{RT} in 2010 induced a later start timing of SPB. When increasing the winds during SPB period, more phytoplankton was taken downward from the surface layer by the enhanced vertical mixing. Meanwhile, more nutrients were pumped upward to the surface layer and supported more net growth of phytoplankton. These two contrary processes led to the independence of the magnitude of SPB on the TKE_{RT} during the SPB period. However, larger TKE_{RT} along with stronger wind resulted in a longer duration of SPB because of more nutrients supply by stronger vertical mixing.

1. Introduction

Oceanic phytoplankton is the basis of the oceanic food web which supports the higher trophic production and fish recruitment (Townsend et al., 1994; Son et al., 2014). It is also regarded as a key factor to modulate the climate change due to its ability of converting carbon dioxide to oxygen through photosynthesis (Falkowski et al., 1998; Brown et al., 2014). Phytoplankton bloom (PB) is defined as the fast growth and accumulation of phytoplankton, which contributes much to the global primary production (Wollast, 1991; Tilstone et al., 2014). Spring phytoplankton bloom (SPB), occurring in different geographical regions (subpolar, temperate and subtropical zones) and in different waters (both deep oceans and shallow seas), was always described by three characteristics, i.e., the start timing (Tian et al., 2011), magnitude (Lips et al., 2014) and duration (Frajka-Williams and Rhines, 2010). The start timing is important for the development of zooplankton and has implications for fish larvae and their stocks (Rey et al., 1987; Platt et al., 2003). The magnitude and duration affected the amount of energy transferred to the higher trophic level (Sigler et al., 2014).

There are two theories explaining the start of SPB. A classical paradigm is the Sverdrup Theory (Sverdrup, 1953), which is also called to be the critical depth concept. At the critical depth, the depth-integrated photosynthesis is equal to the depth-integrated losses of phytoplankton. Hence, SPB can develop only if the upper mixed layer is shallower than the critical depth. In spring of temperate zones, the

* Corresponding author at: College of Environmental Science and Engineering, Ocean University of China, 238 Songling Road, Qingdao 266100, China.
E-mail address: huiwanggao@126.com (H. Gao).

http://dx.doi.org/10.1016/j.csr.2016.06.008
Received 31 December 2015; Received in revised form 1 May 2016; Accepted 15 June 2016
Available online 16 June 2016
0278-4343/ © 2016 Elsevier Ltd. All rights reserved.

upper mixed layer becomes shallower due to the increasing heat flux at sea surface. The light conditions become favorable for photosynthesis. So, the interannual variation of the start timing of SPB is closely related to the development of seasonal stratification, which has been proved useful in many oceans (Kirk, 1994; Navarro et al., 2012; Xu et al., 2013; Zhou et al., 2013; Cherkasheva et al., 2014). However, this critical depth concept has been challenged by several observations. Townsend et al. (1992) found that the start timing of SPB in the Gulf of Marine preceded the onset of vertical water column stratification. Similar observed phenomenon also occurs in the central Yellow Sea (YS) of China (Han et al., 2011). In early spring, SPB usually starts before the formation of the seasonal stratification.

Huisman et al. (1999) provided another theoretical explanation for these observations, i.e., the critical turbulence concept. Before SPB occurs, nutrients in the water are always sufficient. Strong vertical mixing inhibits the accumulation of phytoplankton by taking it to lower water layers where light is limited (Ueyama and Monger, 2005). SPB develops only when the turbulent mixing rates are less than a critical turbulence. Many studies linked the interannual variation of the start timing of SPB with wind and surface heat flux that could influence the vertical mixing of water. Kim et al. (2007) studied the direct relationship between the timing of SPB and wind speed using the satellite data in the East/Japan Sea, and found SPB began 6–15 days after the wind stress weakened. Moreover, Stramska (2005) pointed out that the variations of wind and heat flux determined the start timing of SPB by changing the turbulent kinetic energy supplied from atmosphere to the oceans in the north polar Atlantic. However, only using satellite data, it is difficult to specify the physical dilution and accumulation of phytoplankton when the TKE_{RT} supplied to the ocean varied under different atmospheric forcing, which directly influences the start timing of SPB.

There are no fixed relationships between the interannual variations of the magnitude of SPB and the vertical mixing. By examining the correlation of the magnitude of SPB and vertical mixing during SPB, Ueyama and Monger (2005) found that the large bloom-period wind mixing could increase or reduce the magnitude in the North Atlantic using the satellite observations. This result was proved in some other oceans (Dutkiewicz et al., 2001; Follows and Dutkiewicz, 2001). During the SPB period, phytoplankton grows fast and nutrients are gradually exhausted. The vertical mixing induced by atmospheric forcing could not only determine the physical transport of phytoplankton in the water column, but also influence the nutrient supplies. The balance between the physical and biological processes will determine the magnitude of SPB, which needs to be further studied based on both observations and models. The interannual variations of the duration of SPB attracted less attention compared to those of the start timing and magnitude, and the responses to the vertical mixing has rarely reported.

In this study, the interannual variations of the start timing, magnitude and duration of SPB in the central southern Yellow Sea (SYS) were studied from 2000 to 2014, using the satellite-derived surface chlorophyll-*a* concentration (Chl-*a*). The relationships between the interannual variation of the turbulent kinetic energy forced by winds and heat fluxes and SPB were examined. Moreover, a 1-D physical-biological coupled model was carried out to quantify the influencing mechanism of turbulent kinetic energy on the interannual variation of SPB.

2. Methodology

2.1. Study area

The SYS, located between the mainland of China and the peninsula of Korea, is a marginal sea of the northwest Pacific Ocean, with an average depth of 44 m and an area of 3.8×10^5 km^2. In the coastal shallow area of the SYS, the satellite-derived surface Chl-*a* is greatly overestimated due to the presence of strong resuspension of sediments. So, this study chooses the area between latitudes 34° and 36°N, and longitudes 123° and 125°E in the central SYS, which is almost more than 70 m in depth (square area in Fig. 1). Based on the historical observations, the nutrients from the rivers always influenced the western coastal areas of the SYS (Wei et al., 2011) and the southwestern SYS (32–33°N, 121–123°E) (Li et al., 2014) rather than the study area. So, the terrestrial impacts on the SPB can be neglected. The time series of the satellite surface Chl-*a* and the atmospheric forcing averaged in this area are derived to investigate the interannual variations and their relationship.

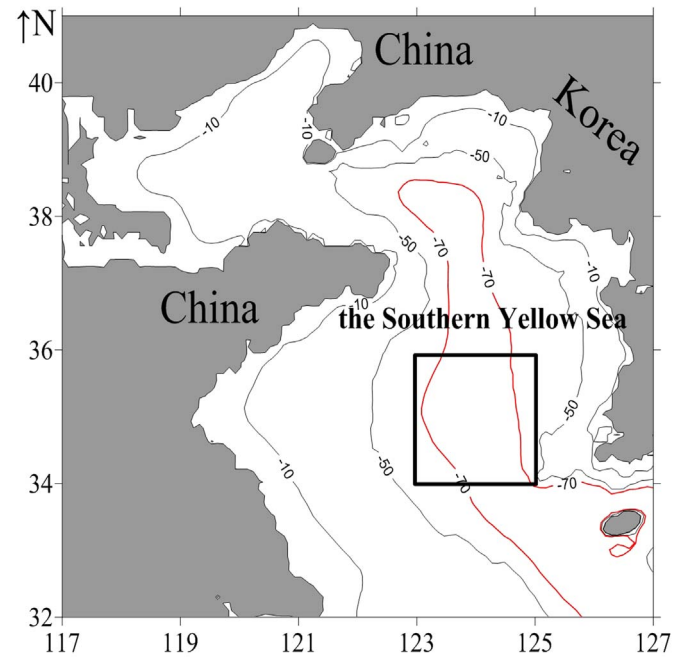

Fig. 1. Bathymetric and geographic map of the YS. The red line is the isobath of 70 m in depth. The square is the study area for the central SYS. (For interpretation of the references to color in this figure legend, the reader is referred to the web version of this article.)

2.2. Data

From 2000 to 2014, the daily sea surface Chl-*a* data are retrieved in the study area. For the period from 2000 to 2007, the surface Chl-*a* are acquired from the SeaWiFS (Sea-viewing Wide Field-of-view Sensor) Level 3 binned data. For the period from 2003 to 2014, similar data are retrieved from MODIS-Aqua (Moderate Resolution Imaging Spectroradiometer) Level 3 binned data. The spatial resolution is 9 km (http://oceancolor.gsfc.nasa.gov/cgi/I3).

The satellite surface Chl-*a* are always overestimated in winter due to the resuspension of sediments in the coastal and even central SYS. However, increases of satellite surface Chl-*a* observed in the central SYS in spring are considered to be the occurrence of SPB (Yamaguchi et al., 2013). In this study, we adopt the satellite surface Chl-*a* data from March 1 to August 31 in each year to study the interannual variation of SPB process in the central SYS, avoiding the data obtained in winter. The two time series are merged into one long time series from 2000 to 2014.

There are differences between the Chl-*a* retrieved from SeaWiFS and MODIS-Aqua (Morel et al., 2007). Before merging the two datasets, the compatibility between the SeaWiFS data and the MODIS-Aqua data is checked during the overlapping period from 2003 to 2007 (excluding data in winter). The correlation between the two datasets is calculated by plotting the daily pixel value from SeaWiFS against that from MODIS-Aqua at the same pixel within the

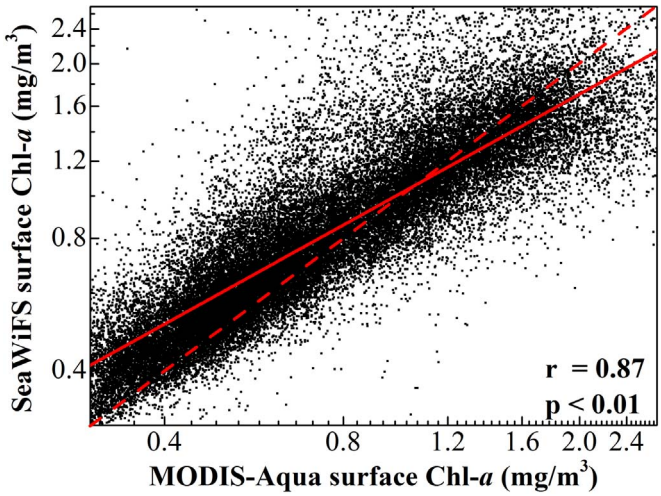

Fig. 2. Comparison of daily surface Chl-*a* retrieved by SeaWiFS and MODIS-Aqua during 2003–2007. The red solid line is the linear regression on the logarithmic scale, and the red dashed line is the 1:1 line. (For interpretation of the references to color in this figure legend, the reader is referred to the web version of this article.)

study area on the same day (Fig. 2). There are 42,194 pairs of concurrent data for the same pixel over the five year, excluding data that differ by more than 3 times the root-mean-square of the deviations. The correlation between the two datasets is represented by the following regression equation:

$$\log(SeaWiFS) = \log(MODISa) \times 0.7504 + 0.0063, (R = 0.87, p < 0.0001),$$

where *SeaWiFS* and *MODISa* are the SeaWiFS and MODIS-Aqua derived surface Chl-*a*, respectively. Correlations were evaluated on log-log scale due to the lognormal distribution of Chl-*a* (Campbell, 1995; Tan et al., 2011; Tan and Shi, 2012).

With this linear regression, the MODIS-Aqua data are converted to those compatible with the SeaWiFS data (He et al., 2013). Then the merged surface Chl-*a* in the study area are averaged to form the time series for the further analyses.

The variation of satellite surface Chl-*a* from March 1 to August 31 is fitted to the Gaussian function of time to get a continuous temporal variation of surface Chl-*a* during the SPB period (Yamada and Ishizaka, 2006; Jo et al., 2007). Gaussian curve is expressed by the equation:

$$Chl(t) = B_0 + Peak \times \exp\left[-\frac{(t - t_m)^2}{2\sigma^2}\right],$$

where B_0 is the background surface Chl-*a*, *Peak* and t_m are the peak value and peak time of the surface Chl-*a*, *t* is the time expressed by Julian day, and σ is the standard deviation of the Gaussian curve. Then, the surface Chl-*a* in January and February are determined by the Gaussian curve. The following analyses are based on the Gaussian curve of each year.

The net heat fluxes and wind speed data from 2000 to 2014 are taken from NCEP/NCAR daily reanalysis data (http://www.esrl.noaa.gov/psd/data/gridded/reanalysis/). The spatial resolution of these data is 1.875°. The data acquired in the study area every day are averaged to serve as the value for the day.

2.3. Determination of SPB characteristics

The start timing, magnitude and duration are three important characteristics of SPB. The threshold method based on the cumulative Chl-*a* is widely used in ocean color data to identify the start timing of SPB (Brody et al., 2013). Based on the Gaussian curve of Chl-*a* in each year, the daily Chl-*a* are cumulatively summed day by day from the 1st day (the beginning of January) to 243rd day (the end of August) of the year to create a time series of cumulative variance. The start timing of SPB is the day when the cumulative value rises to a specific percentage of that of the 243rd day. Among eight thresholds between 5 and 40% (5, 10, 15, 20, 25, 30, 35% and 40%), it is found that only when the threshold is 30%, the start timing of SPB of all the 15 years falls between t_m-σ and t_m. Therefore, the threshold of 30% is adopted. The peak time is when the Chl-*a* reaches to its peak value. The end of SPB is set to be symmetric with the start timing about the peak time. The duration is the time period between the start timing and the end of SPB. The magnitude is defined as the peak value of the surface Chl-*a* during the SPB process, which can be expressed as the maximum value on the Gaussian curve.

2.4. The rate of generation of turbulent kinetic energy (TKE_{RT})

2.4.1. The definition of TKE_{RT}

The vertical mixing of water affects the SPB by influencing the stability of the water column and the nutrients transportation from deep sea water up to the euphotic layer. We use meteorological data to quantify the intensity of vertical mixing in spring in the study area (Stramska, 2005) and test if there is a significant correlation between the vertical mixing and the three characteristics of SPB. According to the bulk mixed layer theories (Kraus and Turner, 1967; Niiler and Kraus, 1977), the vertical mixing is related to the rate of generation of turbulent kinetic mixing (TKE_{RT}). The TKE_{RT} can be quantified in terms of wind stirring and buoyancy forcing as follows:

$$TKE_{RT} = m_1 u^{*3} + m_2 \frac{\alpha g}{\rho c_p} \frac{MLD}{2}(-H_0),$$

where TKE_{RT} is the turbulent kinetic energy, *MLD* is the mixed layer depth, u^* is the wind-induced friction velocity, ρ is the water density, c_p is the specific heat, *g* is the gravitational acceleration, α is the coefficient of logarithmic expansion of ρ as a function of water temperature, and H_0 is the net heat flux. Several previous studies have assumed m_1=1.25 and m_2=1 for negative buoyancy forcing when ocean loses heat to the atmosphere and m_2=0.2 for positive buoyancy forcing when ocean gains heat from the atmosphere (Kraus et al., 1988). The first term on the right side of the equation (*Peak*) indicating the rate of work by the wind is referred to as t_m. The second term on the right side of the equation ($m_2 \frac{\alpha g}{\rho c_p} \frac{MLD}{2}(-H_0)$) representing the rate of potential energy change caused by heat fluxes across sea surface is represented by TKE_H.

The wind always increases TKE_{RT} in the oceanic upper boundary layer. The buoyancy forcing can either increase TKE_{RT} when the water column loses heat to the atmosphere, or reduce TKE_{RT} when the water column becomes stratified owing to the absorption of heat from the atmosphere.

2.4.2. The definition of TKE_{RT} weakening time

The SPB usually starts in late March or early April (Xuan et al., 2012). The daily TKE_{RT} is normalized by dividing the maximum TKE_{RT} in March before the SPB in these 15 years. The mean normalized TKE_{RT} is hereby derived by averaging over all the daily normalized TKE_{RT} in March of the 15 years. The daily anomalies of normalized TKE_{RT} are the differences between the daily TKE_{RT} and the mean normalized TKE_{RT}. Then the CUSUM stands for the cumulative value of the daily anomalies of normalized TKE_{RT}. The TKE_{RT} weakening time is defined as the time when CUSUM curve begins to descend and the decreasing tendency lasts for no less than one week to eliminate the possibility of violent fluctuation. The method has been used to describe the weakening of wind stress in the sub-polar frontal area of the Japan/East Sea (Kim et al., 2007).

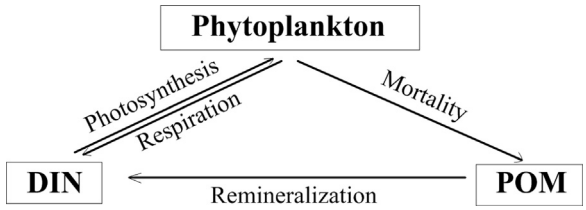

Fig. 3. The Scheme of the biological module.

2.5. The 1-D physical-biological coupled model

2.5.1. Model description

The 1-D physical-biological coupled model comprises a hydrodynamic module and a biological module (Fig. 3). The hydrodynamic module provides the water temperature and vertical mixing coefficient to the biological module. The hydrodynamic module is based on the 1-D Princeton Ocean Model (Blumberg and Mellor, 1987). Three state variables are included in the biological module: dissolved inorganic nitrogen (DIN), one phytoplankton, and particulate organic matter (POM). The biological processes included in the module are shown in Fig. 3. Phytoplankton absorbs DIN for photosynthesis and releases DIN through respiration. The mortalities of phytoplankton contribute to POM, which returns to DIN through remineralization. Parameters used in the model (Table 1) are based on those reported in literatures (Vichi et al., 2004; Tian et al., 2005; Liu et al., 2007; Zhao and Guo, 2011) and made a reasonable modification when debugging and validating the model.

2.5.2. Model configuration and data sources

The water depth in the model is set to be 70 m in the central SYS. There are 40 layers in the vertical direction. Both physical and biological variables are calculated simultaneously at a time step of 108 s. The model is forced by the daily wind, heat fluxes and sea surface salinity, all of which are derived from NCEP reanalysis datasets (http://www.esrl.noaa.gov/psd/data/gridded/reanalysis/).

The model is initialized with the World Ocean Atlas 2013 (WOA2013) that is the climatological monthly mean data with the spatial resolution of 1°(http://www.nodc.noaa.gov/OC5/woa13/woa13data.html). The WOA2013 data in January in the study area are averaged to provide the initial vertical profiles of water temperature, salinity and DIN concentration. The initial concentrations of Chl-*a* and POM are set to be low values.

The numerical simulations consist of five cases, namely, CONTROL, Exp1, Exp2, Exp3 and Exp4. In CONTROL, the climatological atmospheric forcing, including wind, heat fluxes, and solar radiation, are provided to simulate the seasonal cycles of the physical and biological variables. The WOA2013 data in four seasons represented by February, May, August and November are used to validate the modeled vertical profiles of temperature, DIN concentrations. Validation data for seasonal variations of Chl-*a* profiles are from the in situ observations in April, July, November of 2011 and January of 2012 from observations by the authors' research groups.

Exp1 and Exp2 are designed to evaluate the influence of TKE_{RT} before SPB (taking wind-driven TKE for example) on the start timing of SPB. In Exp1, the sea surface forcing are set to be those in 2008. In Exp2, the sea surface heat fluxes and solar radiation are the same as those in Exp1. The water temperature influencing the biological processes is also the model results of Exp1. However, the winds are derived from the values in 2010. So, the calculated vertical diffusivity coefficients are different in Exp1 and Exp2 caused only by the different winds. Exp3 and Exp4 are designed to evaluate the influences of TKE_{RT} (taking wind-driven TKE for example) during the SPB period on the magnitude and duration of SPB. All the forcing conditions in Exp3 and Exp4 are the same as those in CONTROL except the wind during the SPB period. The 15-year mean wind speed during the SPB period is 6.0 m/s. The maximum mean wind speed during SPB period is 8.6 m/s in 2011, while the minimum value is 4.0 m/s in 2014. Therefore, in Exp3, the daily wind speeds adopted during SPB are set as 2.6 m/s larger than that in CONTROL, while in Exp4, the daily wind speeds are set as 2.0 m/s lower.

Table 1
Parameters in the biological module and sensitivities of annual mean surface Chl-*a* to the parameters.

Parameters	Value	References	Variation of Parameter	Sensitivities of annual mean surface Chl-*a*
Maximum specific photosynthetic rate (/day)	1.1	Zhao and Guo, 2011	+50% −50%	0.28 0.40
Characteristic Q_{10} coefficient	2.0	Vichi et al., 2004	+50% −50%	0.06 0.30
Half saturation value for N-limitation (mmol N/m^3)	1.8	Zhao and Guo, 2011	+50% −50%	0.34 0.80
Basal specific respiration rate (/day)	0.05	Tian et al., 2005	+50% −50%	0.04 0.06
Activity respiration fraction	0.14	Tian et al., 2005	+50% −50%	0.12 0.16
Basic lysis rate (/day)	0.1	Liu et al., 2007	+50% −50%	0.60 1.34
Remineralization rate (/day)	0.03	Vichi et al., 2004	+50% −50%	0.58 0.22
Optimal C:Chl quota (mg C/mg Chl-*a*)	50.0	Tian et al., 2005	+50% −50%	1.00 1.00

3. Results

3.1. Validation of satellite-derived Chl-a in the central SYS

The satellite-derived surface Chl-*a* were validated by observations from the literatures and observations by the authors' research groups (Fig. 4). In situ Chl-*a* data were obtained in October and November of 2000 from Deng et al. (2008), in March, April, and September of 2003 from Zhang et al. (2009), in October and November of 2005 from

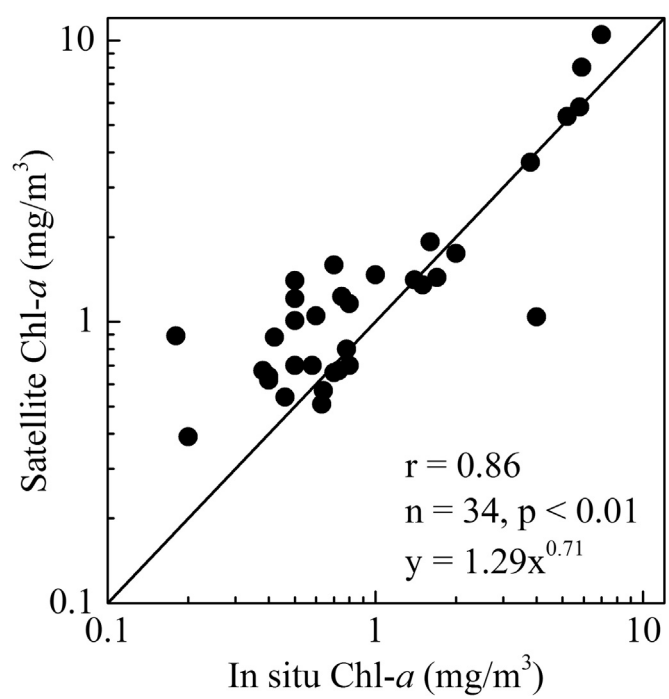

Fig. 4. Comparison of satellite-derived Chl-*a* and in situ Chl-*a*.

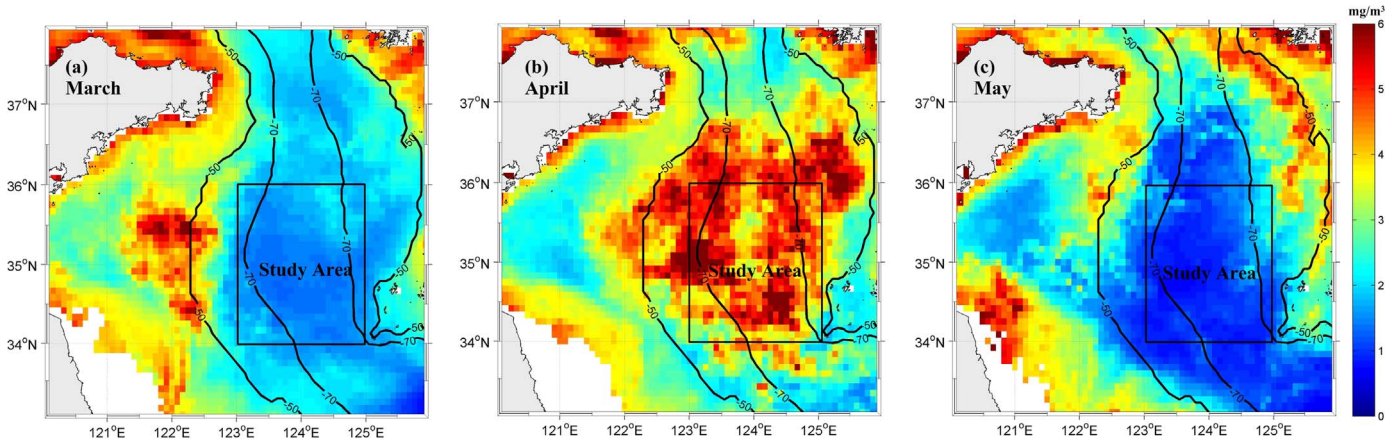

Fig. 5. Spatial distribution of monthly mean surface Chl-*a* in the SYS calculated from all the satellite data in the same month from 2000 to 2014. The colors represent the surface Chl-*a*. The solid lines are the isobaths of 50 m and 70 m. The square is the study area. (For interpretation of the references to color in this figure legend, the reader is referred to the web version of this article.).

Zheng et al. (2006), in June and July of 2006 from Wang et al. (2009), in July and August of 2006 from Fu et al. (2009), in April, October, and November of 2006 and March and August of 2007 from Liu et al. (2015), in April of 2007 from Xuan et al. (2012), in October and November of 2007 from Wei et al. (2013), in April of 2009 from Xuan et al. (2011), in April of 2011 from Wen et al. (2012), in August of 2011 from Liu et al. (2014), and in March, June, and August of 2009, July and October of 2011, October of 2012, June, July, and September of 2013 from observations by the authors' research groups. These data were averaged in the study area. The satellite data were correlated strongly to the in situ Chl-*a*, with a correlation coefficient of 0.86, relationship $y=1.29\times^{0.71}$. Correlations were evaluated on log-log scales due to the lognormal distribution of Chl-*a* (Campbell, 1995).

3.2. Climatological variations of SPB process and TKE_{RT} in the central SYS

The distribution of the surface Chl-*a* are analyzed based on the multi-annual monthly average data (Fig. 5). March is the incubation period of the SPB in the central SYS (Xuan et al., 2011). The surface Chl-*a* in the area with the depth more than 50 m is generally low. In April, the obvious SPB occurs. The surface Chl-*a* is high in the study area, and April is always regarded as the occurrence period. The vanishing period of the SPB in the central SYS is May. However, the Chl-*a* in near-shore areas is generally high throughout the year. The overestimation by the satellite data usually occurs there due to the resuspension of sediments in these shallow regions. The other reason is that nutrients from the river always support vigorous growth of phytoplankton. So, the SPB occurs primarily in deep regions of the central SYS (the study area).

Using the space-average method to process the daily surface Chl-*a* from 2000 to 2014 in the study area (Fig. 1), the climatological SPB process is analyzed (black curve in Fig. 6). The surface Chl-*a* remains low, less than 1.0 mg/m^3, in January and February when the water temperature is low and solar radiation is weak. In March, the surface Chl-*a* increases sharply as the physical environment becomes favorable for photosynthesis. The SPB starts on the 89th day of the year (around March 30), when the cumulative sum (CUSUM) of the surface Chl-*a* (presented by blue curve in Fig. 6) reaches 30% of the CUSUM on the 240th day (the end of August), as defined in Section 2.3. Then, the surface Chl-*a* ascends to its peak value of 2.5 mg/m^3 on the 102nd day of the year (around April 12). The end timing of SPB is the 115th day (around April 25), which is symmetrical with the start timing of SPB about the peak time. The SPB lasts for 26 days, with the magnitude of 2.5 mg/m^3. Then the surface Chl-*a* decreases due to the depletion of nutrients in the euphotic layer and remains low in summer.

The 15-year averaged TKE_H, TKE_W and TKE_{RT} are presented in Fig. 6 (yellow, purple and red curves in Fig. 6). In winter, before the start of SPB, the TKE_H is mostly positive, indicating the intensive loss of heat by the ocean. The TKE_W is higher than that in other seasons due to the intensive winter monsoon. Therefore, the TKE_{RT} of this period is high so that the ocean is well mixed, better pumping up the nutrients to the euphotic layer. However, the strong vertical mixing is not good for the physical accumulation of phytoplankton. Note that during this time of a year, the TKE_H contributes more to TKE_{RT} than TKE_W. In early spring when SPB starts, the TKE_H is sometimes negative and sometimes positive, with the absolute values more than an order of magnitude smaller than the values in winter. The TKE_W also reduces due to the attenuation of the winter monsoon. Consequently, the water column is less disturbed and becomes stable, favorable for the accumulation of phytoplankton. During the period of SPB, the TKE_{RT} remains low. The contribution of TKE_W to TKE_{RT} becomes comparable to those of TKE_H. From the end of SPB to summer, the TKE_H is mostly negative due to the net heat gain by the ocean from the atmosphere. The TKE_{RT} is thus reduced, resulting in the stratification of the water column. The upward transport of nutrients is hindered so that the surface Chl-*a* is low.

3.3. Interannual variations of SPB and TKE_{RT} in the central SYS

3.3.1. Interannual variation of SPB

The variations of the daily surface Chl-*a* from January to June in the 15 years were well described by the Gaussian function (Fig. 7). The 15-year averaged correlation coefficient between the Gaussian curve and the satellite-derived Chl-*a* was 0.76. Three parameters, i.e., *Peak*, t_m and σ, were estimated for each year. The averaged values of *Peak*, t_m and σ in the 15 years were 3 mg/m^3, the 102nd day and 18 days, respectively.

The start timing, magnitude and duration of SPB showed obvious interannual variations in the central SYS (Table 2). The characteristics of SPB in 2006 were greatly different from those of the other 14 years. It started the latest on April 9, lasted for the shortest period of only 8 days and had the largest magnitude of 9.82 mg/m^3. For the other 14 years, the earliest start timing was found in 2008, on March 22 and the latest in 2013, on April 8. The maximum value of the magnitude of SPB was 3.40 mg/m^3 in 2008, nearly doubling the lowest value of 1.73 mg/m^3 in 2009. The 14-year averaged magnitude was 2.64 mg/m^3. The duration of SPB in 2003 and 2008 was shortest, which is 18 days, about half of the longest duration of 38 days found in 2010. The average duration for the 14 years was 26 days. Tan and Shi (2012) attributed the significantly high surface Chl-*a* and primary production in the central SYS in 2006 to the Asian dust rather than the vertical mixing of

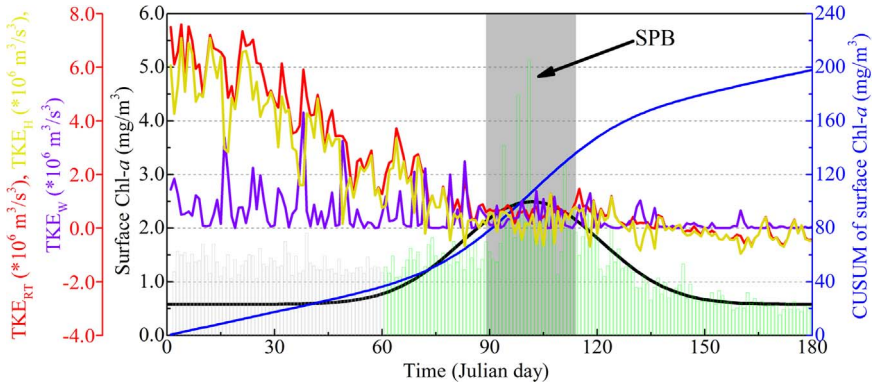

Fig. 6. The climatological variations of TKE_W (purple curve), TKE_H (yellow curve), TKE_{RT} (red curve), daily satellite-derived surface Chl-*a* (gray and green columns). The black line is the Gaussian curve fitting the variation of surface Chl-*a* from March to August (green columns), and the blue curve represents the CUSUM of the surface Chl-*a*. The dark gray area represents the SPB period. (For interpretation of the references to color in this figure legend, the reader is referred to the web version of this article.)

water. So, the year of 2006 was excluded when analyzing the correlation between SPB and TKE_{RT} in the following sections.

3.3.2. Interannual variation of TKE_{RT}

The earliest start timing was the 81st day found in 2008. The average values of TKE_{RT} in one week, two weeks and one month before the 81st day were calculated in each year, namely as $TKE_{RT\text{-}1w}$, $TKE_{RT\text{-}2w}$ and $TKE_{RT\text{-}1m}$. The interannual variations of these three values were analyzed (Fig. 8a). In most years, the $TKE_{RT\text{-}1m}$ was the largest with the 15-year averaged value of 1.9×10^{-6} m^3/s^3, while the $TKE_{RT\text{-}1w}$ was the smallest with the average value of 1.1×10^{-6} m^3/s. The $TKE_{RT\text{-}2w}$ was in between. In winter, strong winter monsoon and atmospheric cooling increased the TKE_{RT}. Consequently, longer averaged time period before the SPB led to stronger TKE_{RT}. However, it is not the case with the years of 2003, 2004, 2010 and 2011, which were probably caused by episodic strong wind event or cold air outbreak in the transition time from winter to spring.

The interannual changing trends of $TKE_{RT\text{-}2w}$ and $TKE_{RT\text{-}1m}$ were almost the same. The values were low in 2002, 2008 and 2013, while relatively higher values occurred in 2001, 2005, 2011 and 2012. The peak values could reach about 3.0×10^{-6} m^3/s^3, while the low values were around zero. The interannual variation of $TKE_{RT\text{-}1w}$ before the SPB was similar to $TKE_{RT\text{-}2w}$ and $TKE_{RT\text{-}1m}$ except the years of 2001 and 2005.

The TKE_{RT} during the SPB remained low in most of the years except 2010 with the value being 2.2×10^{-6} m^3/s^3 (Fig. 8b). The lowest value was -1.2×10^{-7} m^3/s^3, which in 2008. The mean value was 4.8×10^{-7} m^3/s^3, one order smaller than TKE_{RT} before SPB.

In addition to the values of TKE_{RT}, the interannual variation of TKE_{RT} weakening time was also examined (Table 2). The average weakening time was the 78th day (March 19). The earliest weakening time was the 65th day (March 6), found in 2002, which was almost one month earlier than the latest weakening time of the 90th day (March 31) as in 2006.

3.4. Relationship between three characteristics of SPB and TKE

3.4.1. Correlations between the start timing of SPB and TKE

The relationships between the start timing of SPB and $TKE_{RT\text{-}1w}$, $TKE_{RT\text{-}2w}$ and $TKE_{RT\text{-}1m}$ were studied (Fig. 9). The start timing of SPB was most related to the $TKE_{RT\text{-}1w}$ with the correlation coefficient of 0.63 (Fig. 9a). The positive coefficient showed that larger TKE_{RT} before the SPB induced later start timing of SPB. The smaller correlation coefficient of 0.57 and a larger p-value indicated a weaker relationship between the start timing of SPB and $TKE_{RT\text{-}2w}$ (Fig. 9b). However, the p-value larger than 0.1 suggested that the start timing of SPB was not related to $TKE_{RT\text{-}1m}$ (Fig. 9c). Hence, the start timing of SPB depended on the value of TKE_{RT} shortly before the SPB. Once TKE_{RT} became small, the water column was stable for the accumulation of phytoplankton and led to the start of SPB.

The TKE_{RT} weakening time and the start timing of SPB exhibited a significantly positive correlation with a coefficient of 0.9 (Fig. 9d). It was suggested that the earlier TKE_{RT} weakened, the earlier SPB started. There was also a time lag between the TKE_{RT} weakening time and the start timing of SPB. The SPB started 5–20 days after the weakening of TKE_{RT}. The minimum time lag is in the year 2011, which is 5 days, while the maximum is in 2013, 20 days (Table 2).

In early spring before the SPB started, the large TKE_{RT} caused strong vertical mixing, which cannot maintain a stable water column for the accumulation of phytoplankton. Thus, the larger TKE_{RT} before the SPB, the later the SPB started. Once the TKE_{RT} weakened, the SPB started. However, they did not occur simultaneously. It took some days from the weakening of TKE_{RT} to the start of SPB. The time lag indicated that the water column needed some time to be stable enough after the weakening of TKE_{RT}.

The variation of TKE_{RT} was caused by different wind and surface heat fluxes. Fig. 10 showed the correlations between the anomolies of TKE_H, TKE_W and TKE_{RT} and one week before the SPB. The interannual variation of TKE_{RT} significantly related to that of TKE_W, indicated by a positive coefficient of 0.87 (Fig. 10a). However, the variation of TKE_{RT} was not relevant to the TKE_H indicated by a large p-value more than 0.1 (Fig. 10b). It was suggested that the interannual variation of wind determined the start timing of SPB by influencing the stability of the water column.

3.4.2. Correlations between the magnitude and duration of SPB and TKE

When calculating the correlation coefficient between the interannual variation of the SPB and the TKE_{RT} during the SPB, the p-value was larger than 0.1, which indicated that there was no obvious correlation between the two items (Fig. 11a). Strong vertical mixing tended to make the Chl-*a* vertically diluted. Consequently, large TKE_{RT} was not good for the accumulation of phytoplankton in the euphotic layer and did not support a large magnitude of SPB. In contrast, small TKE_{RT} failed to bring sufficient nutrients from nutrient-rich lower water up to the euphotic layer to support the growth of phytoplankton, although weak vertical mixing was good for the physical accumulation of phytoplankton. Therefore, there were no significantly negative or positive correlation between the TKE_{RT} and the magnitude of SPB.

The positive correlation coefficient (r=0.66) between the interannual variation of the duration of SPB and TKE_{RT} during the SPB period (Fig. 11b) indicated that stronger TKE_{RT} during the SPB period could support a longer duration of SPB. As mentioned in the previous section, stronger TKE_{RT} did not necessarily support a higher magnitude of SPB, especially when the physical dilution of phytoplankton overwhelmed the biological promotion. However, stronger TKE_{RT}

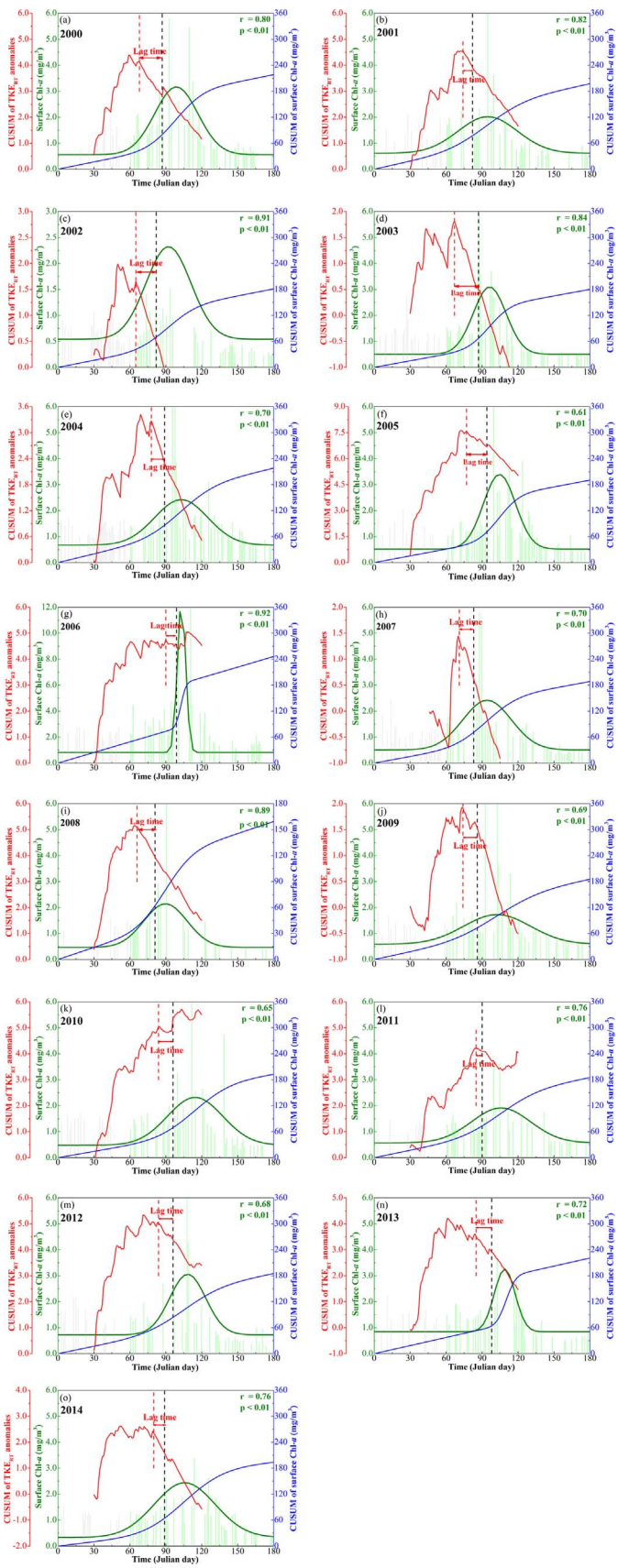

Fig. 7. The variations of surface Chl-*a* (green curve), CUSUM of surface Chl-*a* (blue curve) and CUSUM of TKE_{RT} anomalies (red curve) from 2000 to 2014. The gray and green columns are the daily satellite-derived surface Chl-*a*. The green curve is the Gaussian curve fitting the variations of surface Chl-*a* from March to August. The black dashed line is the start timing of SPB, and the red dashed line represents the weakening timing of TKE_{RT}. The difference between the two timing is the lag time. (For interpretation of the references to color in this figure legend, the reader is referred to the web version of this article.)

Table 2
The interannual variations of the start timing, magnitude, duration of SPB, the weakening time of TKE_{RT} and the lag time from weakening time of TKE_{RT} to the start timing of SPB.

Year	Start timing (Julian day)	Magnitude (mg/m^3)	Duration (day)	Weakening time of TKE_{RT} (Julian day)	Lag time (day)
2000	87	3.17	24	67	20
2001	82	2.02	26	74	8
2002	82	2.32	20	65	17
2003	87	3.10	18	67	20
2004	89	2.42	28	78	11
2005	94	3.40	22	88	6
2006	99	9.82	8	90	9
2007	83	2.42	22	76	7
2008	81	3.40	18	66	15
2009	86	1.73	34	74	12
2010	96	2.32	38	85	11
2011	90	1.92	30	85	5
2012	96	3.06	24	85	11
2013	98	3.26	22	86	12
2014	89	2.44	34	80	9

successively pumped up nutrients to support the growth of phytoplankton, delayed the end of SPB and thus maintained a longer SPB.

In order to evaluate the contribution of wind and heat fluxes to the variation of TKE_{RT} during the SPB, the correlation coefficients between TKE_{RT} and TKE_H and TKE_W were calculated (Fig. 12). The correlation coefficient between TKE_{RT} and TKE_W reached up to 0.97 (Fig. 12a), while the variation of TKE_{RT} was not relevant to that of TKE_H (Fig. 12b). It was suggested that the interannual variation of winds during SPB, rather than heat fluxes, determined the magnitude and duration of the SPB by influencing the stability of the water column and nutrients supply.

4. Discussion

It was found that the TKE_{RT} had some relationship with the three characteristics of SPB in the previous section. The TKE_{RT} influenced the SPB by changing the vertical mixing in the water. The variation of Chl-*a* in the surface layer was caused partly by the vertical mixing of phytoplankton, which was referred as the physical process. In addition, nutrients pumped up to the euphotic layer by the vertical mixing promoted the growth of phytoplankton, which was referred as the biological process. It was difficult to evaluate the contributions of the two processes caused by TKE_{RT} to the variations of SPB process only by calculating the correlation coefficients between them. So, in this section, a 1-D physical-biological coupled model was used to study the influences of TKE_{RT} on the interannual variation of the start timing, magnitude and duration of SPB. The winds were changed to represent the variations of TKE_{RT} in the numerical experiments, and the responses of the three characteristics of SPB were estimated. The detail definitions of the numerical runs were in the section of methodology. Moreover, the variations of the surface Chl-*a* caused by vertical mixing (i.e., the contribution of the physical process) and net growth of phytoplankton (i.e., the contribution of the biological process) were also calculated in each numerical experiments and compared to discuss the influencing mechanism of TKE_{RT} on the three characteristics of SPB.

4.1. Model validations

Before quantitatively analyzing the model results, the model sensitivity to parameters uncertainties was estimated. The sensitivity of a predicted state variable to selected parameter was quantified as a factor $s = \frac{|\Delta A / A|}{|\Delta B / B|}$, where A was the annual mean surface Chl-*a* and B was

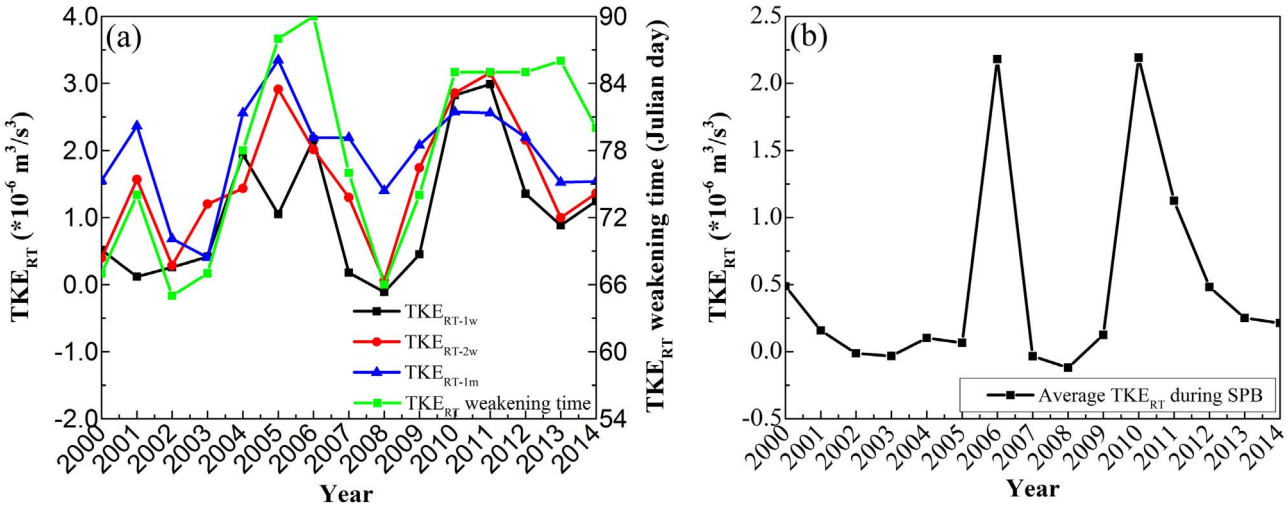

Fig. 8. The variations of $TKE_{RT\text{-}1w}$ (black line), $TKE_{RT\text{-}2w}$ (red line), $TKE_{RT\text{-}1m}$ (blue line) before SPB, the weakening time of TKE_{RT} (a), and the variation of average TKE_{RT} during SPB (b). (For interpretation of the references to color in this figure legend, the reader is referred to the web version of this article.)

the value of one model parameter. ΔA was the variation of A when one parameter varied at ΔB. In this study, the value of any selected parameter was increased and decreased by 50% from the standard value listed in Table 1. Sixteen experiments were carried out to calculate the sensitivities (Table 1). Only in one case, the sensitivity was bigger than 1. More than 60% of the sensitivities are ≦0.5. So, the model results were robust if these parameters were changed moderately. The model results were more sensitive to the basic lysis rate and the half saturation value of DIN. The sensitivity of the value of C/Chl-*a* was a constant (s=1). The C/Chl-*a* was not a parameter using in the model calculation, but a coefficient to convert the unit of the results from C to Chl-*a*. This ratio showed variable due to changes in light,

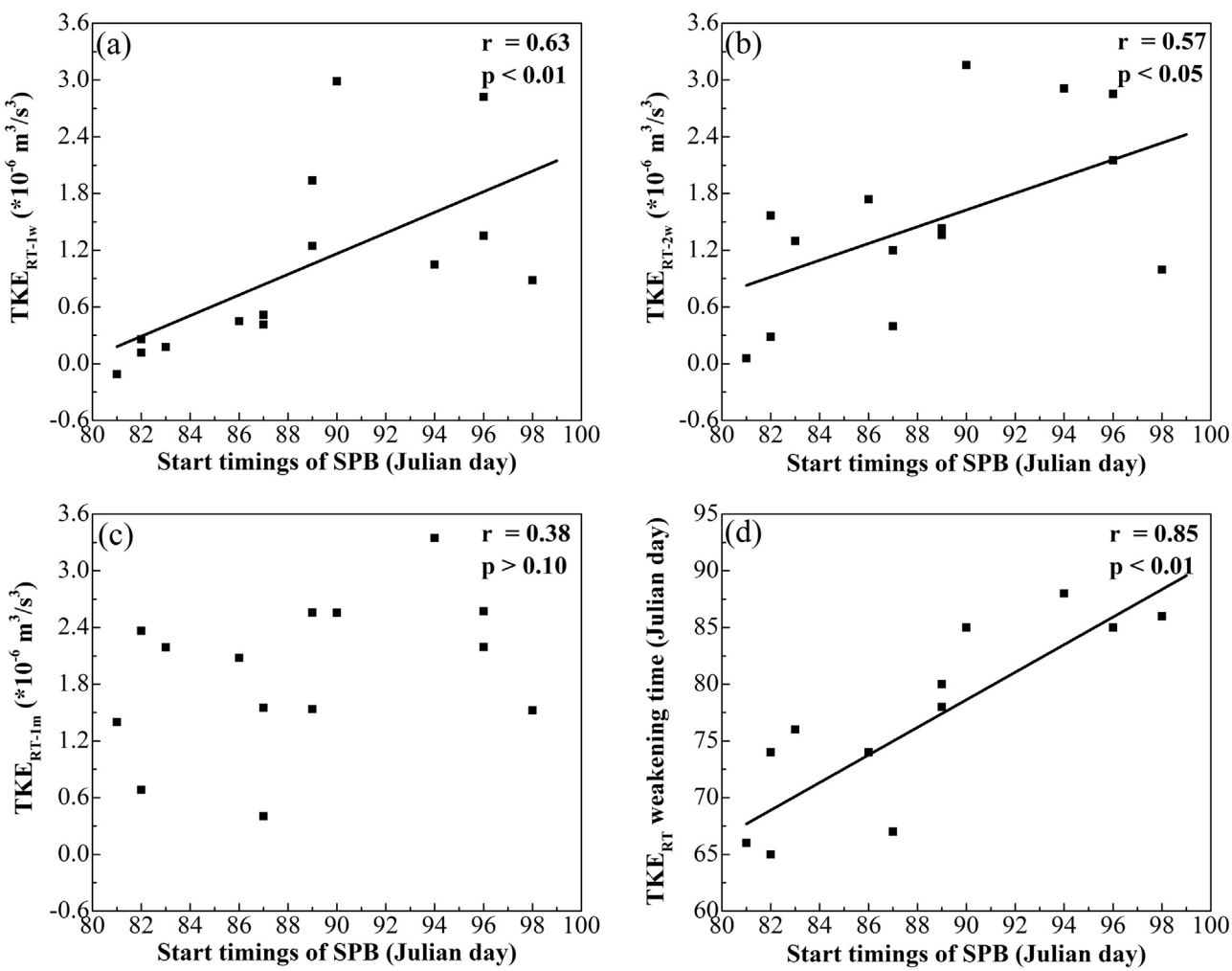

Fig. 9. Correlations between $TKE_{RT\text{-}1w}$ (a), $TKE_{RT\text{-}2w}$ (b), $TKE_{RT\text{-}1m}$ (c), the weakening time of TKE_{RT} (d) and the start timing of SPB.

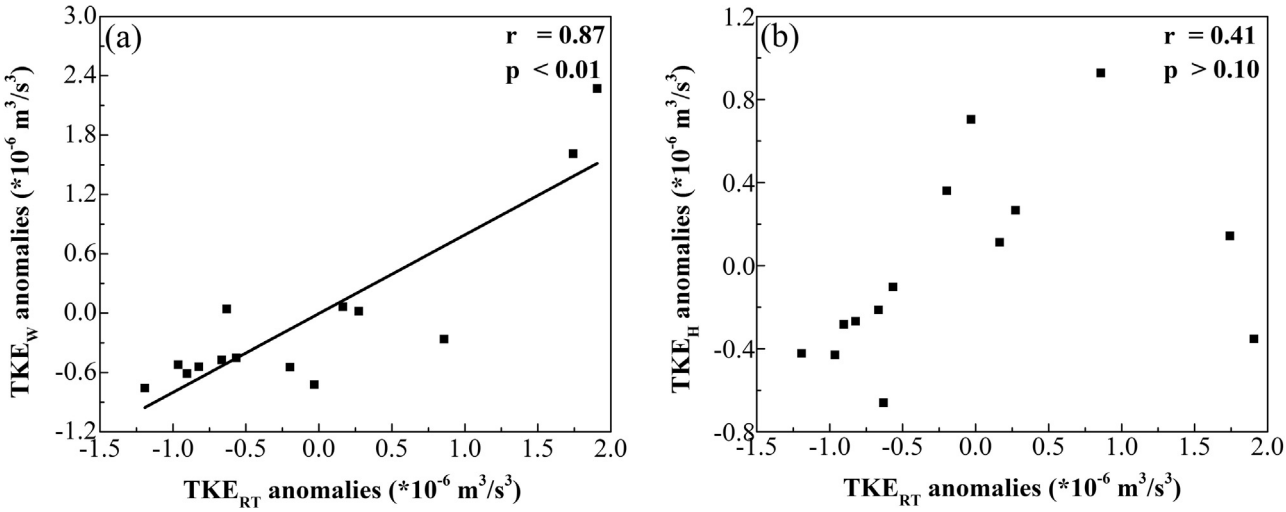

Fig. 10. Correlations between TKE_W anomalies (a), TKE_H anomalies (b) and TKE_{RT} anomalies in one week before SPB.

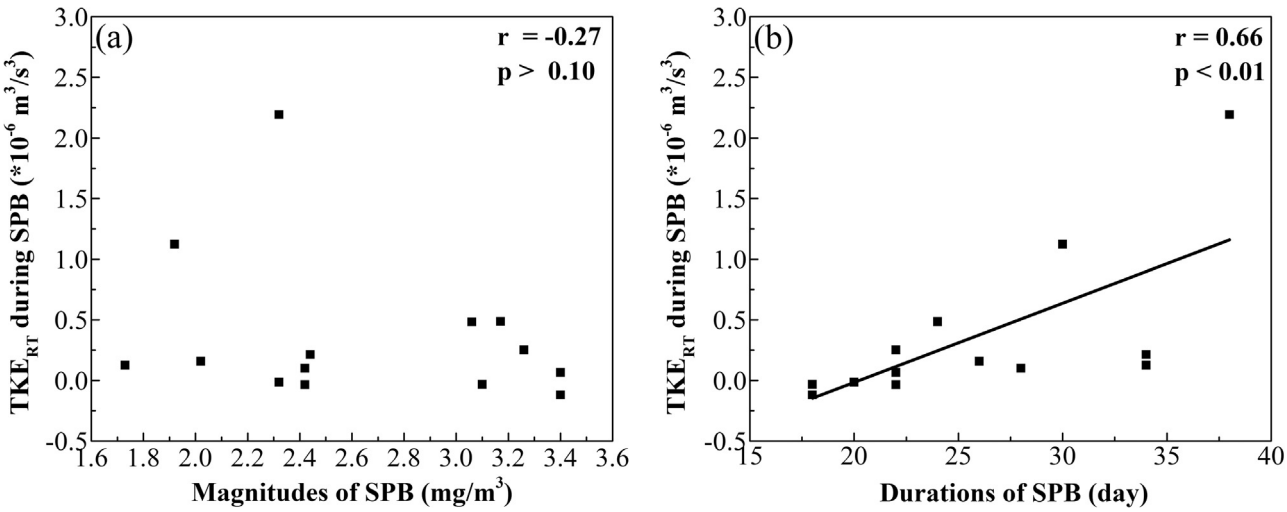

Fig. 11. Correlations between magnitudes (a), durations of SPB (b) and TKE_{RT} during SPB.

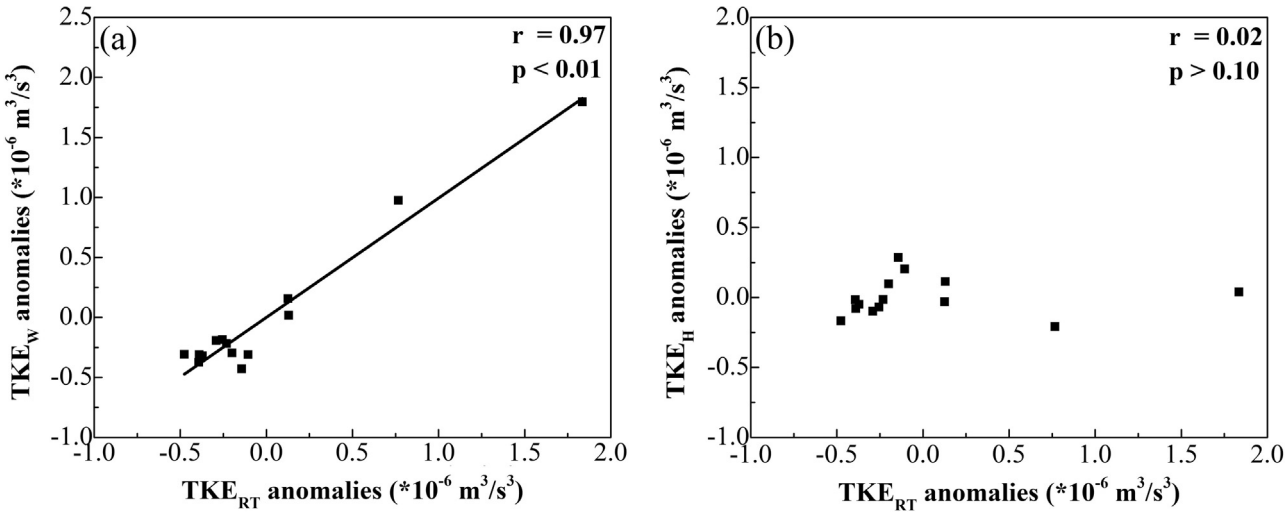

Fig. 12. Correlations between TKE_W anomalies (a), TKE_H anomalies (b) and TKE_{RT} anomalies during SPB.

nutrients conditions and phytoplankton species (Geider et al., 1997). The value was set to be 50 according to some previous model studies in East China Seas (Tian et al., 2005; Liu et al., 2007; Zhao and Guo, 2011).

The modeled results for water temperature, DIN concentration and Chl-*a* were in good agreement with the observations (Fig. 13). In winter, all physical and biochemical elements were mixed well by the strong winter monsoon. The water temperature remained lowest

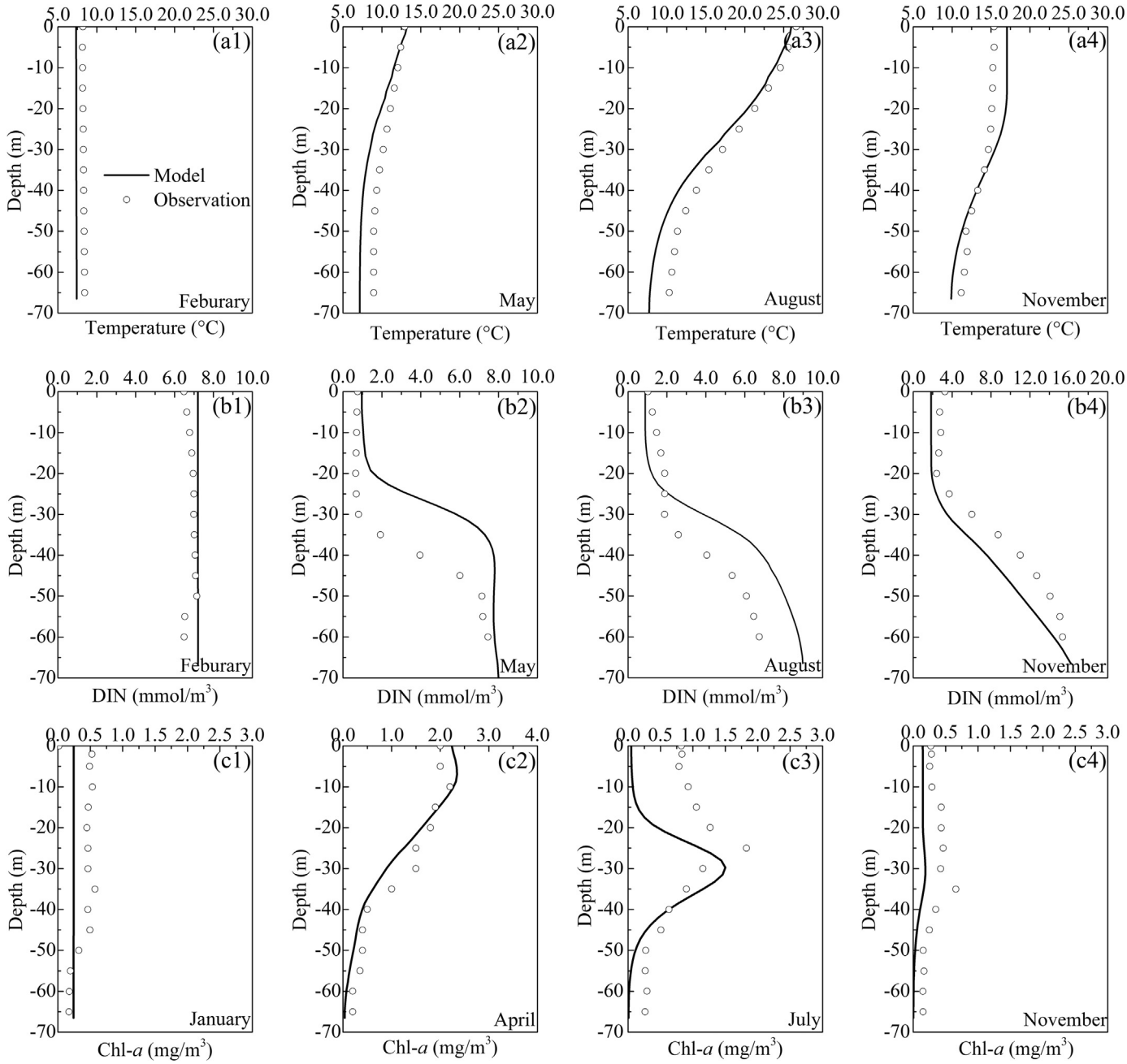

Fig. 13. Comparison of modeled seasonal variations of the vertical profiles of temperature, DIN concentrations and Chl-*a* (solid line in the figures) with the observations (circles in the figures). The observations of temperature and DIN concentrations are from WOA2013 data in February, May, August and November. Observations of Chl-*a* are the in-situ observations in April, July, November of 2011 and January of 2012.

throughout the year due to the loss of heat to the atmosphere. DIN was sufficient in the water column, however the growth of phytoplankton was limited by the low temperature and weak solar radiation, as a result, Chl-*a* was very low. In spring, the environment is favorable for the growth of phytoplankton, so Chl-*a* fast increased in the upper layer which was SPB phenomenon. The growth of phytoplankton was still limited by light under the euphotic layer, and Chl-*a* remained low there. The vertical profile of DIN concentration showed an inverse shape comparing with that of Chl-*a*. In summer, the water was stratified indicated by the profile of temperature. DIN was exhausted by phytoplankton in surface layer. Under the influences of both nutrient and light, the subsurface chlorophyll maximum formed which was indicated by the profile of Chl-*a*. In fall, the water column tended to be well mixed again due to the surface cooling and strengthening of wind.

4.2. The influence of TKE_{RT} on the start timing of SPB

After model validations, two numerical experiments (Exp1 and Exp2) were carried out to evaluate the influence of TKE_{RT} on the start timing of SPB. In Exp1, the annual cycles of vertical profiles of water temperature, vertical mixing coefficient, DIN concentration and Chl-*a* in 2008 were simulated. Compared with the atmospheric forcing in Exp1, only the winds were replaced by that of 2010 in Exp2. However, the water temperatures used in the biological module were set to be the same as those in Exp1. So, the only difference between Exp1 and Exp2 was the vertical mixing coefficient forced by different TKE_{RT}.

SPB in the central SYS always started in late March to early April. Before the start timing of SPB, the average wind speed in March of 2008 was 5.5 m/s, which was much smaller than that in 2010 (9.0 m/s) (Fig.14 (a)). As a result, the variations of TKE_{RT} in Exp1 and Exp2 were

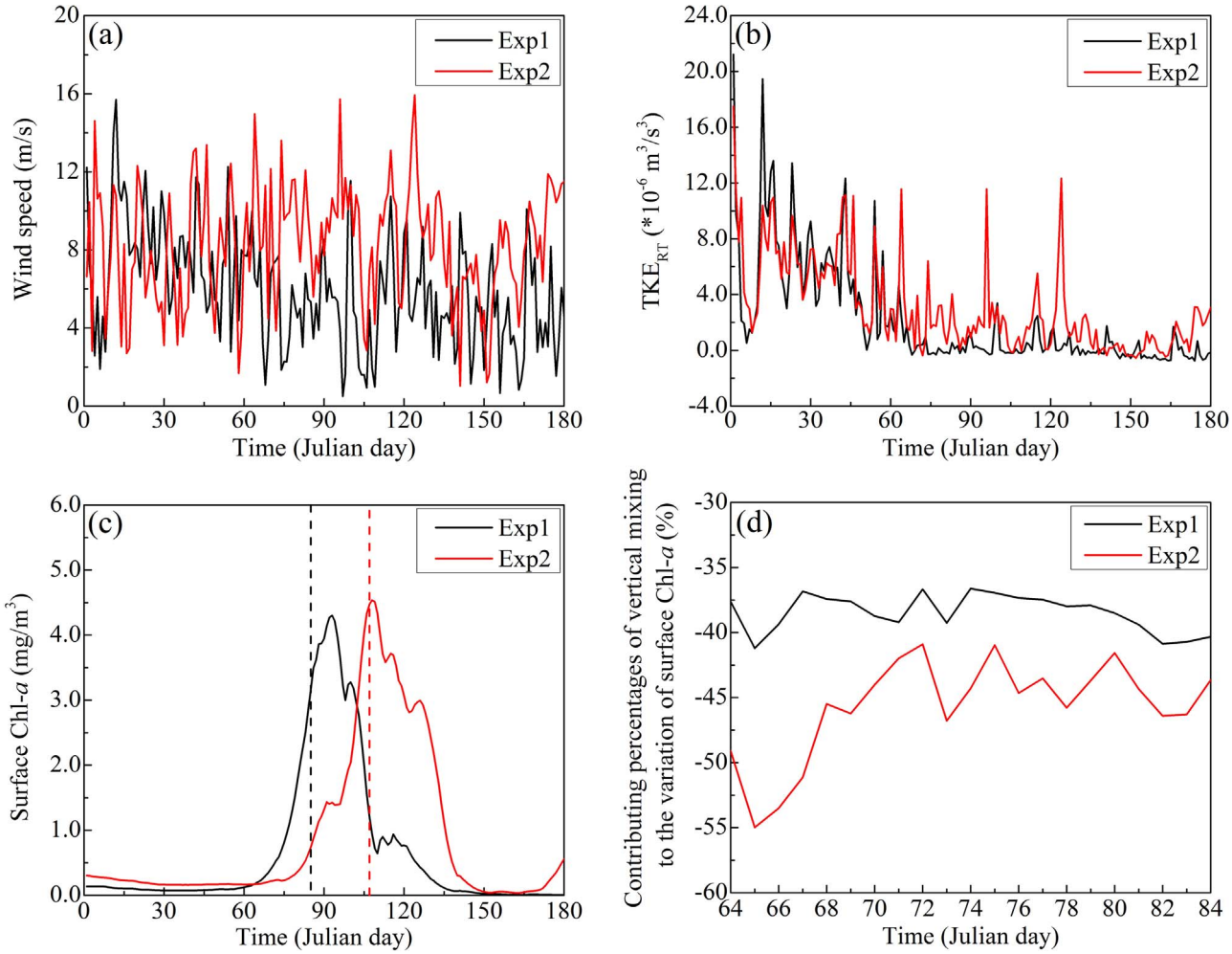

Fig. 14. The variations of wind speed (a), TKE_{RT} (b), modeled surface Chl-*a* (c) and the contributing percentages of the vertical mixing to the variation of modeled surface Chl-*a*. The black and red solid lines represent the variables in Exp1 and Exp2, respectively. The black and red dashed lines in (c) represent the start timing of SPB in Exp1 and Exp2, respectively. (For interpretation of the references to color in this figure legend, the reader is referred to the web version of this article.)

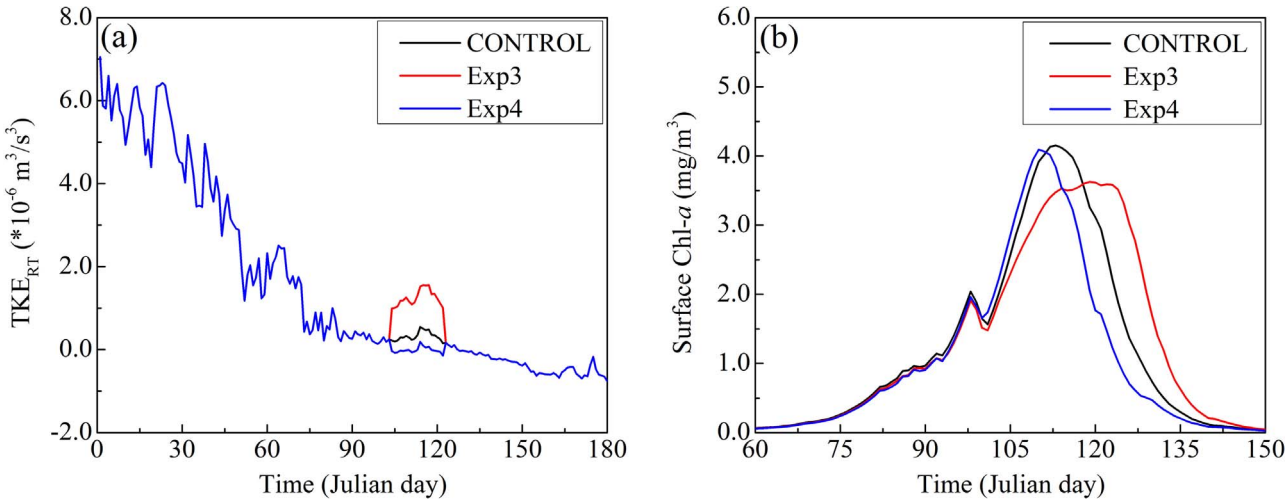

Fig. 15. The variations of TKE_{RT} (a) and modeled surface Chl-*a* (b) in three numerical experiments. The black, red and blue solid lines represent the variables in CONTROL, Exp3 and Exp4, respectively. (For interpretation of the references to color in this figure legend, the reader is referred to the web version of this article.)

quite different. The TKE_{RT} in the two experiments were both high in winter (January and February). In March, the TKE_{RT} in Exp2 was still high due to the strong winds (red curve in Fig.14 (b)), while the TKE_{RT} in Exp1 decreased to be around zero (black curve in Fig.14(b)), indicating less energy input to the water from the atmosphere. Consequently, the vertical mixing in water in Exp1 was weaker than that in Exp2 in March before the SPB started.

The modeled surface Chl-*a* in the two experiments exhibited different variations (Fig.14 (c)). SPB started on the 85th day in Exp1, while on the 105th day in Exp2. On the 64th day, the surface Chl-*a* in

Table 3
The contributions of the physical and biological process to the variation of surface Chl-*a* and DIN flux integrated from the start timing to the peak time of CONTROL.

	CONTROL	Exp3	Exp4
Biological process (mg/m^3)	8.8	9.2	7.8
Physical process (mg/m^3)	−7.0	−7.6	−6.1
DIN flux (mmol/m^2)	48.3	56.0	43.5

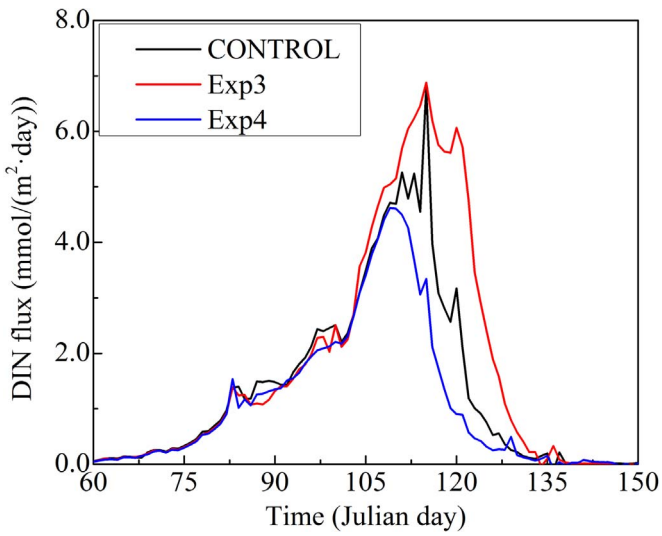

Fig. 16. The variations of DIN transported upward to the surface layer in CONTROL (black line), Exp3 (red line) and Exp4 (blue line). (For interpretation of the references to color in this figure legend, the reader is referred to the web version of this article.)

Exp1 started to exceed that in Exp2, and the difference gradually increased, leading to the earlier start timing in Exp1. In order to evaluate the contribution of the vertical mixing to the start of SPB, the contributing rate of the surface Chl-*a* variation caused by vertical mixing to the total surface Chl-*a* variation were calculated (Fig.14(d)). From the 64th day to the start timing in Exp1 (the 85th day), the contributing percentages in both experiments maintained negative, indicating downward physical transport of phytoplankton from the surface layer. In addition, the absolute values of the contributing rate in Exp2 were always larger than those in Exp1. It was suggested that larger vertical mixing in Exp2, which was caused by larger TKE_{RT} was not favorable for the accumulation of phytoplankton and thus led to a later start timing of SPB.

4.3. The influence of TKE_{RT} on the magnitude and duration of SPB

Three numerical experiments (CONTROL, Exp3 and Exp4) were carried out to examine the influences of TKE_{RT} on the magnitude and duration of SPB. The model configurations of these experiments were shown in Section 2.5.2. Based on the modeled variation of surface Chl-*a* in CONTROL, the start and end timing of SPB were calculated to be the 104th day and the 122nd day. The average wind speeds during SPB were increased to reach the maximum average value in the 15 years in Exp3 and decreased to be the minimum average value in Exp4. As a result, The TKE_{RT} in the three experiments varied with the change of winds (Fig. 15 (a)). The SPB processes in the three experiments were consequently different in terms of magnitude and duration.

The magnitudes of SPB were 4.2 mg/m^3, 3.6 mg/m^3 and 4.1 mg/m^3 in CONTROL, Exp3 and Exp4, respectively (Fig. 15 (b)). The magnitude of SPB seemed to be not related to the TKE_{RT}, which was also suggested by the data analyses in the result section. From the start timing (the 104th day) to the peak time (the 113th day) of SPB of CONTROL, the contributions of the physical (vertical mixing) and biological (net growth) processes to the variations of Chl-*a* were estimated in the three experiments (Table 3). The variations of surface Chl-*a* caused by the physical process were −7.0, −7.6 and −6.1 mg/m^3 in CONTROL, Exp3 and Exp4, respectively. The negative contributions of the physical process in the three experiments suggested that the vertical mixing took phytoplankton downward to reduce the Chl-*a* in the surface layer. The absolute values of the physical contributions in the three experiments were consistent with the magnitude of TKE_{RT}. The largest TKE_{RT} in Exp3 led to the largest physical contribution to the variations of surface Chl-*a*. In comparison, in Exp4, the vertical mixing took the least phytoplankton downward from the surface layer due to the smallest TKE_{RT}. However, the contributions of the biological process to the variations of surface Chl-*a* in the three experiments changed in a contrary tendency. The net growth of phytoplankton in CONTROL, Exp3 and Exp4 were 8.8, 9.2 and 7.8 mg/m^3, respectively. The modeled amounts of DIN transported up to the surface layer from the start timing (the 104th day) to the peak time (the 113th day) of SPB in CONTROL, Exp3 and Exp4 were 48.3, 56.0 and 43.5 mmol/m^2, respectively (Table 3). The consistent tendency of the net growth and the nutrient transport in the three experiments indicated that the larger vertical mixing took more nutrients up to the surface layer to support more net growth of phytoplankton.

The durations of SPB in CONTROL, Exp3 and Exp4 were 18, 24 and 12 days, respectively, which was consistent with the magnitude of TKE_{RT} during the SPB. The variations of DIN transported up to the surface layer in the three experiments were calculated (Fig. 16), and the average values during the SPB (from the 104th to the 122nd day) were 3.9, 5.4 and 2.9 mmol/(m^2 day) in CONTROL, Exp3 and Exp4, respectively. Larger TKE_{RT} in Exp3 brought more DIN to the surface layer through stronger vertical mixing, resulting in a longer SPB, and vice versa in Exp4.

5. Conclusions

The SPB has great contribution to the primary production in the local food chain in the central SYS. It always occurs in late March to early April, when the strong winter monsoon begins to attenuate (Xuan et al., 2011; Yuan et al., 2014). The satellite-derived daily surface Chl-*a* in spring were fitted by the Gaussian function from 2000 to 2014, and the three characteristics of SPB were determined by the Gaussian curve. The start timing, magnitude and duration of SPB all experienced obvious interannual variations. After TKE_{RT} has weakened for some time, SPB started. The start timing of SPB was positively related to TKE_{RT} in a short period before SPB. The relationship between the magnitude of SPB and the TKE_{RT} during SPB was comparably complicated. Larger TKE_{RT} during the SPB did not definitely induce a larger magnitude of SPB, but can prolong the duration of SPB. It was noted that the TKE_W, instead of the TKE_H, contributed to TKE_{RT} when influencing the start timing and duration of SPB.

In addition, a 1-D physical-biological coupled model was carried out to quantify how TKE_{RT} influenced SPB. Larger TKE_{RT} before SPB delayed the start timing of SPB by transporting more phytoplankton downward from the surface layer, i.e., the water column was unstable for the accumulation of phytoplankton. When increasing/decreasing the wind during the SPB period, more/less phytoplankton was taken downward from the surface layer by the physical process. Meanwhile, more/less nutrients were pumped up to the surface layer by the enhanced/weakened vertical mixing and supported more/less net growth of phytoplankton. These two contrary processes led to the independence of the magnitude of SPB on the TKE_{RT} during SPB. However, larger TKE_{RT} resulted in a longer duration of SPB because of more adequate nutrients supply by stronger vertical mixing.

The findings in this study indicate that the mechanism controlling the interannual variations of SPB in continental shelf seas, such as the YS, is the critical turbulence concept (Huisman et al., 1999), which is

different from those in open oceans explained by the Sverdrup theory (Sverdrup, 1953).

Acknowledgments

We thank NASA for providing the satellite-derived Chl-*a* datasets and the atmospheric forcing data. This research is funded in part by the National Natural Science Foundation of China under the contract of 41106007, the NSFC-Shandong Joint Fund for Marine Science Research Centers under the contract of U1406403, the China Postdoctoral Science Foundation under the contract of 2014M560575 and the National Basic Research Program ("973" program) of China under the contract of 2011CB403606. Two anonymous reviewers and editor provided detailed and constructive comments that strengthened the manuscript.

References

Blumberg, A.F., Mellor G.L., 1987. A description of a three-dimensional coastal ocean circulation model. Three-dimensional coastal ocean models, pp. 1–16.
Brody, S.R., Lozier, M.S., Dunne, J.P., 2013. A comparison of methods to determine phytoplankton bloom initiation. J. Geophys. Res.: Oceans 118, 2345–2357.
Brown, C.W., Schollaert, Uz, S., Corliss, B.H., 2014. Seasonality of oceanic primary production and its interannual variability from 1998 to 2007. Deep Sea Res. I 90, 166–175.
Campbell, J.W., 1995. The lognormal distribution as a model for bio-optical variability in the sea. J. Geophys. Res. 100, 13237-12254.
Cherkasheva, A., Bracher, A., Melsheimer, C., Koberle, C., Gerdes, R., Nothig, E.-M., Bauerfeind, E., Boetius, A., 2014. Influence of the physical environment on polar phytoplankton bloom: a case study in the Fram Strait. J. Mar. Syst. 132, 196–207.
Deng, C.M., Yu, Z.G., Yao, P., Chen, H.T., Xue, C.Y., 2008. Size-fractionated phytoplankton in the East China and Southern Yellow Seas and its environmental factors in autumn 2000. Period. Ocean Univ. China 38, 791–798, (in Chinese with English abstract).
Dutkiewicz, S., Follows, M., Marshall, J., 2001. Interannual variability of phytoplankton abundances in the North Atlantic. Deep Sea Res. II 48, 2323–2344.
Falkowski, P.G., Barber, R.T., Smetace, V., 1998. Biogeochemical controls and feedbacks on ocean primary production. Science 281, 200–206.
Follows, M., Dutkiewica, S., 2001. Meteorological modulation of the North Atlantic spring bloom. Deep Sea Res. II 49, 321–344.
Frajka-Williams, E., Rhines, P.B., 2010. Physical controls and interannual variability of the Labrador Sea spring phytoplankton bloom in distinct regions. Deep Sea Res. I 57, 541–552.
Fu, M.Z., Wang, Z.L., Sun, P., Li, Y., Li, R.X., 2009. Spatial distribution characteristics and the environmental regulation mechanisms of phytoplankton chlorophyll *a* in Southern Yellow Sea during Summer 2006. Acta Ecol. Sin. 29, 5366–5375, (in Chinese with English abstract).
Geider, R.J., MacIntyre, H.L., Kana, T.M., 1997. Dynamic model of phytoplankton growth and acclimation: responses of the balanced growth rate and the chlorophyll a: a carbon ratio to light, nutrient-limitation and temperature. Mar. Ecol. Progress. Ser. 148, 187–200.
Han, J., Wei, H., Zhao, L., Shi, Y., Shi, J., Zhang, G., 2011. The effects of horizontal advection on the spring bloom of phytoplankton in the central Southern Huanghai Sea. Acta Oceanol. Sin. 30, 24–31.
He, X., Bai, Y., Pan, D., Chen, C.-T.A., Cheng, Q., Wang, D., Gong, F., 2013. Satellite views of the seasonal and interannual variability of phytoplankton blooms in the eastern China seas over the past 14 yr (1998–2011). Biogeosciences 10, 4721–4739.
Huisman, J., Oostveen, P., Weissing, F.J., 1999. Critical depth and critical turbulence: two different mechanisms for the development of phytoplankton blooms. Limnol. Oceanogr. 44, 1781–1788.
Jo, C.O., Lee, J.-Y., Park, K.-A., Kim, Y.H., Kim, K.-R., 2007. Asian dust initiated early spring bloom in the northern East/Japan Sea. Geophys. Res. Lett., 34.
Kim, H.-c, Yoo, S., Oh, I.S., 2007. Relationship between phytoplankton bloom and wind stress in the sub-polar frontal area of the Japan/East Sea. J. Mar. Syst. 67, 205–216.
Kirk, 1994. Light and Photosynthesis in Aquatic Ecosystems. Cambridge University Press, Cambridge, 509.
Kraus, E.B., Turner, J.S., 1967. A one-dimensional model of the seasonal thermocline. Tellus 19, 98–105.
Kraus, E.B., Bleck, R., Hanson, H.P., 1988. The inclusion of a surface mixed layer in a layer in a large-scale circulation model, In: Nihoul, J.C.J., Jamart, B.M. (Eds.), Small Scale Turbulence and Mixing in the Ocean, pp. 51–62.
Li, H.M., Zhang, C.S., Han, X.R., Shi, X.Y., 2014. Changes in concentrations of oxygen, dissolved nitrogen, phosphate, and silicate in the southern Yellow Sea, 1980–2012: sources and seaward gradients. Estuar. Coast. Shelf Sci. 163, 44–55.
Lips, I., Runk, N., Kikas, V., Meerits, A., Lips, U., 2014. High-resolution dynamics of the spring bloom in the Gulf of Finland of the Baltic Sea. J. Mar. Syst. 129, 135–149.
Liu, C.Y., Liu, H.H., Yang, G.P., Wang, L.L., Zhang, S.H., 2014. Relationships among the distributions of acrylic acid, marine environmental factors and chlorophyll a in the Yellow Sea Cold Water Mass in summer. Adv. Earth Sci. 29, 361–368, (in Chinese with English abstract).
Liu, X., Huang, B.Q., Huang, Q., Wang, L., Ni, X.B., Tang, Q.S., Sun, S., Wei, H., Liu, S.M., Li, C.L., Sun, J., 2015. J. Sea Res. 95, 45–55.
Liu, Z., Wei, H., Bai, J., Zhang, J., Liu, D.Y., Liu, S.M., 2007. Nutrients seasonal variation and budget in Jiaozhou Bay, China : a 3-D physical-biological coupled model study. Water Air Soil Pollut.: Focus 7, 607–623.
Morel, A., Huot, Y., Gentili, B., Werdell, P.J., Hooker, S.B., Franz, B.A., 2007. Examining the consistency of products derived from various ocean color sensors in open ocean (Case 1) waters in the perspective of a multi-sensor approach. Remote Sens. Environ. 111, 69–88.
Navarro, G., Caballero, I., Prieto, L., Vazquez, A., Flecha, S., Huertas, I.E., Ruiz, J., 2012. Seasonal-to-interannual variability of chlorophyll-*a* bloom timing associated with physical forcing in the Gulf of Cadiz. Adv. Space Res. 50, 1164–1172.
Niiler, P.P., Kraus, E.B., 1977. One-dimensional models of the upper ocean. In: Kraus, E. B. (Eds.), Modelling and Predictions of the Upper Layer of the Ocean, pp. 143–172.
Platt, T., Fuentes-Yaco, C., Frank, K.T., 2003. Spring algal bloom and larval fish survival. Nature 423, 398–399.
Rey, F., Skjoldal, H.R., Slagstad, D., 1987. Primary production in relation to climate changes in the Barents Sea. In: Bergen, L. (Ed.), The Effect of Oceanographic Conditions on Distribution and Population Dynamics of Commercial Fish Stocks in the Barents Sea. Institute of Marine Research, Norway, 29–46.
Sigler, M.F., Stabeno, P.J., Eisner, L.B., Napp, J.M., Mueter, F.J., 2014. Spring and fall phytoplankton blooms in a productive subarctic ecosystem, the eastern Bering Sea, during 1995–2011. Deep SeA Res. II: Top. Stud. Oceanogr. 109, 71–83.
Son, S.H., Wang, M.H., Harding, L.W., Jr, 2014. Satellite-measured net primary production in the Chesapeake Bay. Remote Sens. Environ. 144, 109–119.
Stramska, M., 2005. Interannual variability of seasonal phytoplankton blooms in the north polar Atlantic in response to atmospheric forcing. J. Geophys. Res., 110.
Sverdrup, H.U., 1953. On conditions for the vernal blooming of phytoplankton. J. Cons. Perm. Int. Pour L'Explor. Mer 18, 287–295.
Tan, S.C., Shi, G.Y., Shi, J.H., Gao, H.W., Yao, X.H., 2011. Correlation of Asian dust with chlorophyll and primary productivity in the coastal seas of China during the period from 1998 to 2008. J. Geophys. Res. 116, G02029.
Tan, S.C., Shi, G.Y., 2012. The relationship between satellite-derived primary production and vertical mixing and atmospheric inputs in the Yellow Sea cold water mass. Cont. Shelf Res. 48, 138–145.
Tian, T., Wei, H., Su, J., Chung, C., 2005. Simulations of annual cycle of phytoplankton production and the utilization of nitrogen in the Yellow Sea. J. Oceanogr. 61, 343–357.
Tian, T., Su, J., Floser, G., Wiltshire, K., Wirtz, K., 2011. Factors controlling the onset of spring blooms in the German Bight 2002–2005: Light, wind and stratification. Cont. Shelf Res. 31, 1140–1148.
Tilstone, G.H., Miller, P.I., Brewin, R.J.W., Priede, I.G., 2014. Enhancement of primary production in the North Atlantic outside of the spring bloom, identified by remote sensing of ocean colour and temperature. Remote Sens. Environ. 146, 77–86.
Townsend, D.W., Keller, M.D., Sieracki, M.E., Ackleson, S.G., 1992. Spring phytoplankton blooms in the absence of vertical water column stratification. Nature 360, 59–62.
Townsend, D.W., Cammen, L.M., Holligan, P.M., Campbell, D.E., Pettigrew, N.R., 1994. Causes and consequences of variability in the timing of spring phytoplankton blooms. Deep-Sea Res. I 41, 747–765.
Ueyama, R., Monger, B.C., 2005. Wind-induced modulation of seasonal phytoplankton blooms in the North Atlantic derived from satellite observations. Limnol. Oceanogr. 50, 1820–1829.
Vichi, M., Baretta, J.W., Baretta-Bekker, J.G., 2004. European Regional Seas Ecosystem Model III, Review of the biogeochemical equations. Documentation Release Version
Wang, Z.H., Shi, X.Y., Zhang, C.S., Liang, S.K., Wang, L.S., 2009. Primary study on characteristics of distribution of chlorophyll *a* in the Yellow Sea and East China Sea. Prog. Fish. Sci. 30, 120–126, (in Chinese with English abstract).
Wei, Q.S., Yu, Z.G., Ran, X.B., Zang, J.Y., 2011. Characteristics of the western coastal current of the Yellow Sea and its impacts on the material transportation. Adv. Earth Sci. 26, 145–156, (in Chinese with English abstract).
Wei, Q.S., Fu, M.Z., Li, Y., Wang, B.D., Yu, Z.G., 2013. Observation of the seasonal evolution of DO, chlorophyll a maximum phenomena and nutrient accumulating in the southern HuangHai (Yellow) Sea Cold Water Mass area 35, pp. 143–154. (in Chinese with English abstract)
Wen, F., Sun, X.X., Zheng, S., Luo, X., Feng, Q.Y., Sun, S., 2012. Oceanol. Limnol. Sin. 43, 438–444, (in Chinese with English abstract).
Wollast, R., 1991. The coastal organic carbon cycle: Fluxes, sources and sinks. In: Mantoura, R.F.C., et al. (Eds.), Ocean Margin Processes in Global Change, Dahlem Workshop Reports, pp. 365–381.
Xu, Y., Cahill, B., Wilkin, J., Schofield, O., 2013. Role of wind in regulating phytoplankton blooms on the Mid-Atlantic Bight. Cont. Shelf Res. 63, 26–35.
Xuan, J.L., Zhou, F., Huang, D.J., Wei, H., Liu, C.G., Xing, C.X., 2011. Physical processes and their role on the spatial and temporal variability of the spring phytoplankton bloom in the central Yellow Sea. Acta Ecol. Sin. 31, 61–70.
Xuan, J.L., Zhou, F., Huang, D.J., Zhu, X.H., Xing, C., Fan, X., 2012. Modelling the timing of major spring bloom events in the central Yellow Sea. Estuar. Coast. Shelf Sci. 113, 283–292.
Yamada, K., Ishizaka, J., 2006. Estimation of interdecadal change of spring bloom timing, in the case of the Japan Sea. Geophys. Res. Lett., 33.
Yamaguchi, H., Ishizaka, J., Siswanto, E., Baek Son, Y., Yoo, S., Kiyomoto, Y., 2013. Seasonal and spring interannual variations in satellite-observed chlorophyll-a in the Yellow and East China Seas: new datasets with reduced interference from high concentration of resuspended sediment. Cont. Shelf Res. 59, 1–9.
Yuan, C.Y., Wang, Y.H., Wei, H., 2014. Estimating the budgets of nutrients for phytoplankton bloom in the central Yellow Sea using a modified lower tropic

ecosystem model. Ocean. Coast. Sea Res. 13, 1–12.
Zhang, F., Li, C.L., Sun, S., Wu, Y.L., Ren, J.P., 2009. Distribution patterns of chlorophyll *a* in spring and autumn in association with hydrological features in the southern Yellow Sea and northern East China Sea. Chin. J. Oceanogr. Limnol. 27, 784–792.
Zhao, L., Guo, X.Y., 2011. Influence of cross-shelf water transport on nutrients and phytoplankton in the East China Sea: a model study. Ocean Sci. 7, 27–43.
Zheng, G.X., Song, J.M., Dai, J.C., Wang, Y.M., 2006. Distributions of chlorophyll *a* and carbon fixed strength of phytoplankton in autumn of the southern Huanghai Sea waters. Acta Oceanol. Sin. 28, 109–118, (in Chinese with English abstract).
Zhou, F., Xuan, J.L., Huang, D.J., Liu, C., Sun, J., 2013. The timing and the magnitude of spring phytoplankton blooms and their relationship with physical forcing in the central Yellow Sea in 2009. Deep-Sea Res. II 97, 4–15.